NRL Memorandum Report 4040

Correlations of Crack Branching Properties with Mott Fragmentation Parameters in Hypereutectoid Steels

R. J. WEIMER

Composite Materials Branch
Materials Science and Technology Division

AND

H. C. ROGERS

Materials Engineering Department
Drexel University

July 16, 1979

NAVAL RESEARCH LABORATORY
Washington, D.C.

SECURITY CLASSIFICATION OF THIS PAGE (When Data Entered)

REPORT DOCUMENTATION PAGE

READ INSTRUCTIONS BEFORE COMPLETING FORM

1. REPORT NUMBER: NRL Memorandum Report 4040
2. GOVT ACCESSION NO.
3. RECIPIENT'S CATALOG NUMBER

4. TITLE (and Subtitle): CORRELATIONS OF CRACK BRANCHING PROPERTIES WITH MOTT FRAGMENTATION PARAMETERS IN HYPEREUTECTOID STEELS.
5. TYPE OF REPORT & PERIOD COVERED: Interim report on a continuing NRL problem.
6. PERFORMING ORG. REPORT NUMBER

7. AUTHOR(s): R. J. Weimer and H. C. Rogers*
8. CONTRACT OR GRANT NUMBER(s)

9. PERFORMING ORGANIZATION NAME AND ADDRESS: Naval Research Laboratory, Washington, DC 20375
10. PROGRAM ELEMENT, PROJECT, TASK AREA & WORK UNIT NUMBERS: 61153N-22; RR022-04-41; NRL Problem F04-37.101

11. CONTROLLING OFFICE NAME AND ADDRESS: Department of the Navy, Office of Naval Research, Arlington, Virginia 22217
12. REPORT DATE: July 16, 1979
13. NUMBER OF PAGES: 45

14. MONITORING AGENCY NAME & ADDRESS (if different from Controlling Office)
15. SECURITY CLASS. (of this report): UNCLASSIFIED
15a. DECLASSIFICATION/DOWNGRADING SCHEDULE

16. DISTRIBUTION STATEMENT (of this Report)

Approved for public release; distribution unlimited.

17. DISTRIBUTION STATEMENT (of the abstract entered in Block 20, if different from Report)

18. SUPPLEMENTARY NOTES

*Drexel University, Philadelphia, PA

19. KEY WORDS (Continue on reverse side if necessary and identify by block number)

Crack branching	Microbranching
Fragmentation	Explosive loading
Dynamic fracture	Stress intensity factors
Hackle	Frangibility

20. ABSTRACT (Continue on reverse side if necessary and identify by block number)

When brittle metals are subjected to blast loads, they tend to shatter into a large number of very small particles. The number and size of the particles generated by such an explosive process is well-characterized by the semi-empirical cumulative distribution function of Mott. This function, however, contains no information regarding either the manner of break-up or the reason for a particular distribution. The present experimental investigation was undertaken to clarify the role played by dynamic material properties in the ultimate distribution of particle sizes when brittle metals fracture under

(Continues)

DD FORM 1 JAN 73 1473 EDITION OF 1 NOV 65 IS OBSOLETE
S/N 0102-014-6601

SECURITY CLASSIFICATION OF THIS PAGE (When Data Entered)

20. Abstract (Continued)

explosive loads. The phenomenology of brittle fragmentation was examined previously, and a simple model was developed utilizing the concept of crack branching. Using statistical arguments to establish relationships between the energies associated with crack branching and the Mott parameters that characterize the particle distribution, that model predicts that the average mass of a particle from the shattered body is proportional to the fourth power of the crack branching stress intensity factor. To examine the physical relationships between material properties and particle size distributions from blast-loaded structures, two hypereutectoid steels (FS-01 and HF-1) were heat-treated to a number of brittle conditions and evaluated in terms of static tensile properties, plane strain fracture toughness, crack branching behavior, and explosive fragmentation. The distribution parameters did not correlate with strength, toughness, or hardness, but the coarseness of the particles appeared to increase with increasing tensile elongation. The ratio $(K_H/K_{IC})^{3.4}$ was experimentally determined to be linearly related to the average particle mass in reasonably good agreement with the model prediction, where K_H is the dynamic stress intensity factor for incipient microbranching (hackle).

CONTENTS

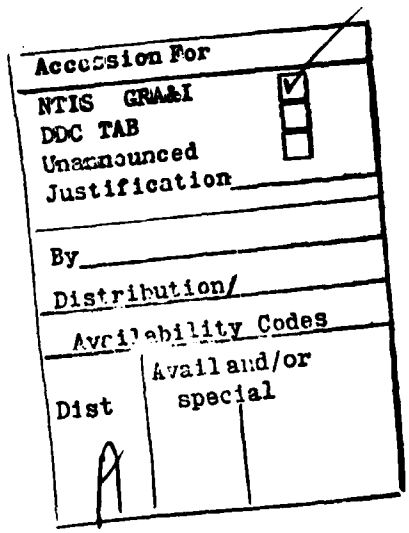

CORRELATIONS OF CRACK BRANCHING PROPERTIES WITH MOTT FRAGMENTATION PARAMETERS IN HYPEREUTECTOID STEELS

INTRODUCTION

For the past several decades, the major concern of analytical and experimental fracture mechanics has been the definition of those conditions that precipitate crack instability in structures. Much recent interest has focused upon the conditions that govern the propagation behavior of dynamic cracks. The impetus for this shift has been provided by the need to improve crack arrest properties of materials, particularly those used in the power and transportation industries. Another aspect of material behavior dominated by crack propagation characteristics rather than by crack initiation conditions, however, is the susceptibility of high-strength materials to shatter rather than simply to yield or to rupture. Such phenomena are characterized by complex interactive networks of simultaneously propagating fractures marked by frequent crack bifurcation events.

N.F. Mott considered the problem of natural fragmentation of metals due to blast loading and subsequently proposed a dynamic model of the fracture of an explosively-loaded ductile metal ring assuming a time-dependent probability of random fracture after a critical strain had been reached in the ring.[1] From this, the form of the particle size distribution can be determined empirically. When the resultant distribution of particle sizes is analyzed, the frequency of occurrence of particular masses follows a cumulative distribution described by a simple exponential relationship:

$$N_m = N_o \exp\left(-\sqrt{m/\mu}\right) \qquad (1)$$

where N_m = total number of particles having mass greater than m, and N_o and μ are experimentally determined parameters representing the total number of particles and half the average mass of the particles.

This relationship describes the explosive break-up of ductile metals quite well. However, Mott's model is based upon instantaneous rupture of thin rings and uses the root-mean-square scatter of the static fracture strain as the criterion for generating a particular particle size distribution. It is, therefore, somewhat surprising to find that equation (1) also describes the distribution of particle

Note: Manuscript submitted May 16, 1979.

sizes that results from the explosive loading of extremely brittle thick-walled cylinders. It is a well-known fact that cracks in highly stressed brittle materials frequently bifurcate; therefore, the stress intensity factor for crack branching in a brittle material should be expected to be functionally related to the statistical parameters that describe the resultant explosive break-up of the material.

On the basis of preliminary analyses of the possible relationships between crack branching stress intensity factor (K_{IB}) and the statistical Mott parameters, Weimer and Rogers [2] suggested that the average particle mass after break-up should be proportional to the fourth power of K_{IB}. They reported experimental results for two hypereutectoid steels which indicated the exponent to be 4.55 ($\pm$ 0.17). However, subsequent experiments and corrections to the stress analysis reduced this exponent to 3.03 ($\pm$ 0.65) with even greater intuitive uncertainty than this standard deviation would indicate, because fully developed branch cracks seldom, if ever, occurred in some of the material conditions tested.

The objective of this investigation is to clarify the role played by dynamic fracture properties of a brittle metal in the distribution of particle sizes that result when this metal is subjected to blast loads. To accomplish this end, a simple model of the explosive shatter of a metal cylinder has been constructed and described in detail elsewhere.[3] Probabilistic arguments were used to demonstrate that the well-established Mott cumulative distribution function could be formally extracted from energy considerations of crack branching phenomena. It was concluded that the average mass and total number of particles from a shattered body did indeed bear fourth-power relationships to the ratio of the crack branching stress intensity factor to the plane strain fracture toughness of a given material. However, the notion of what constitutes crack branching in the explosive loading environment was revised to include hackle, or incipient bifurcation, and experiments were conducted to evaluate this approach.

EXPERIMENTAL PROCEDURE

Selection of Materials: Two hypereutectoid steels were selected for this investigation. One is FS-01 steel (0.92 C, 0.30 Si, 1.15 Mn, 0.50 W, 0.50 Cr, 0.20 V), a fine-grained oil hardening tool steel. The other is HF-1 steel (1.08 C, 0.90 Si, 1.88 Mn), a relatively large-grained silico-manganese steel. FS-01 steel was selected because rather simple thermal treatments could be expected to produce the high strength and hardness levels at which it was anticipated that crack branching could be easily and consistently produced. In addition, the nominal composition was similar to that of the steel used by Anthony [4] in his crack branching investigations. Because of the paucity of experimental data on crack branching in metals, it was considered important at the outset to have some basis for comparison of metallurgical effects.

HF-1 steel was selected because of extensive experience with particle size distributions arising from explosive loading. It was also valuable to have established heat treatment schedules for producing desired distributions in order to economize on experimental design.

Materials Characterization: The materials used in this program were acquired from commercial sources. The FS-01 steel was available both in 4.8 mm thick surface-ground plate stock and 63.5 mm diameter round bar stock, while the HF-1 steel was available only in 4 x 4 RCS (10 cm x 10 cm round-corner-square) bar stock. The heat treatments selected for this investigation were such that the hardness values obtained for FS-01 steel spanned the range obtained by Anthony and in addition included one condition of considerably greater ductility than he utilized. It was also required that the HF-1 steel be heat-treated to conditions identical to those obtained in prior work [5] so that the explosive tests need not be repeated for that material. The actual selection was predicated on the availability of fragments recovered from the earlier HF-1 tests as well as by the large spread in size distribution parameters. The designations and schedules for final heat treatments are listed in Table 1. These designations are retained throughout this work and are used to identify material and its condition. The four FS-01 heat treatments produce very fine-grained tempered martensites at several strength levels. The isothermal treatments of HF-1 cause proeutectoid carbides to precipitate at the grain boundaries. Moreover, the austenitizing temperatures are sufficiently high for A and C that significant grain growth occurs. The resultant microstructures are tempered martensite matrices with carbide networks along prior austenite grain boundaries.

Conventional engineering mechanical properties were measured in accordance with ASTM specifications, including tensile properties,[6] hardness, [7] and fracture toughness.[8] The 0.2% offset yield strength, ultimate tensile strength, and percent elongation in a 51 mm gage length were measured using pin-loaded flat tensile specimens. Tests were conducted at room temperature (~22C) at strain rates of 10^{-4} sec^{-1}. Hardness was measured using the C-scale of a standard Rockwell Hardness Tester. The plane strain fracture toughness was measured at room temperature using single-edge-notch tension specimens that were pin-loaded quasistatically. A summary of all mechanical properties measured is presented in Table 2.

Explosive Testing: Selection of explosives is based upon the nature of the task to be performed. If the requirement is heat, deformation, or simply lifting or heaving ability, the explosive must have a large total work capacity, which is simply a high caloric output per gram of explosive. On the other hand, when the requirement is for high shattering effects, the explosive must have a high rate of delivery of that caloric output. The shattering power of an explosive is termed brisance and is linearly related to the detonation rate (9). Since the expressed intent of this work is to investigate shattering

TABLE 1. HEAT TREATMENT SCHEDULES AND DESIGNATIONS

FS-01(A)	HF-1(A)
Preheat to 538C	927C, 1 hour
Transfer to 800C, 1 hour	Transfer to 760C, 1 hour
Marquench	Oil quench
Temper at 191C, 2 hours	Temper at 482C, 1 hour
Air Cool	Air Cool

FS-01(B)	HF-1(B)
Preheat to 538C	774C, 1 hour
Transfer to 800C, 1 hour	Oil quench
Marquench	Temper at 593C, 1 hour
Temper at 274C, 2 hours	Air Cool
Air Cool	

FS-01(C)	HF-1(C)
Preheat to 538C	982C, 1 hour
Transfer to 800C, 1 hour	Transfer to 760C, 1 hour
Marquench	Oil quench
Temper at 333C, 2 hours	Temper at 649C, 1 hour
Air Cool	Air Cool

FS-01(D)

Preheat to 538C
Transfer to 800C, 1 hour
Marquench
Temper at 438C, 2 hours
Air Cool

TABLE 2. MECHANICAL PROPERTIES[(a)] OF FS-01 AND HF-1 STEELS AFTER HEAT TREATMENT

Heat Treatment Designation	0.2% Offset Yield Strength (MPa)	Ultimate Tensile Strength (MPa)	Percent Elongation (in 51 mm)	Rockwell C-Scale Hardness R_c	Plane-Strain Fracture Toughness K_{IC} (MPa$\sqrt{m}$)
FS-01(A)	2570 (±55)	2709 (±165)	1.2 (±0.7)	61.6 (±0.6)	21.7 (±0.5)
FS-01(B)	2036 (±48)	2303 (±14)	3.8 (±0.6)	56.1 (±0.5)	24.4 (±2.1)
FS-01(C)	1777 (±24)	1937 (±22)	5.1 (±0.6)	52.3 (±0.7)	31.4 (±1.8)
FS-01(D)	1520 (±16)	1616 (±13)	6.5 (±0.3)	47.4 (±0.5)	57.3 (±5.8)
HF-1(A)	1233 (±11)	1316 (±23)	1.3 (±0.1)	42.7 (±0.3)	32.5 (±1.0)
HF-1(B)	949 (± 6)	1214 (± 5)	10.9 (±0.4)	37.3 (±0.6)	37.5 (±4.0)
HF-1(C)	760 (± 5)	1038 (±12)	6.7 (±0.3)	30.0 (±0.0)	40.3 (±3.3)

(a) Based on at least three tests and stated as the mean value (± one standard deviation).

effects in brittle metals, Composition B was selected as the test explosive. Composition B is a derived or secondary high explosive consisting of 64% cyclotrimethylene trinitramine (RDX) and 36% trinitrotoluene (TNT). It has an initial density of 1.71 g/cm^3, a detonation velocity of 8.01 mm/μs which is supersonic with respect to the metal, and a peak explosion pressure of approximately 30 GPa (more than 4,000,000 psi).

Three test cylinders were fabricated for each material condition listed in Table 1. They were machined directly from the bar stock to dimensions slightly greater than shown in Figure 1 which shows the geometry of a test cylinder when charged with explosive. After heat treatment, each cylinder was surface ground to final dimensions and shipped to Denver Research Institute where it was loaded with explosive, detonated, and partially recovered under service contract DAAA25-72-R-0236. The C/M ratio (charge mass to cylinder mass) was held constant at approximately 0.3.

Composition B is a cast explosive. It was extended beyond the cylinder ends to approximate more closely a plane wave when the detonation front reaches and departs the cylinder. The taper simply facilitates removal of the end cap used in casting.

A soft partial recovery system was used to collect particles of the shattered cylinder as shown in Figure 2. This technique has evolved from experience and direct comparison with total recovery systems; the results are equivalent but simpler to obtain. The system is called soft in relation to recovery in sand or sawdust. Basically it consists of a fragment shield and recovery tank located far enough from the exploding cylinder that the charge can be considered as a point source. In the shield there is a window that subtends an angle of 30^o at the source and allows fragments to pass through to the recovery tank. The latter is filled with water and covered with a high density urethane foam pad as shown.

Trisodium phosphate (Na_3PO_4) and sodium nitrite ($NaNO_2$) were added to water at a rate of 1.9 grams of each per liter of water to inhibit rusting of the recovered particles. The actual recovery is on a framed 50 mesh brass screen submerged in the tank and covering the entire bottom.

The particles are removed from the recovery screen by an electromagnet, dried, and sorted into size groups by sieving; after counting they are batch-weighed and returned for analysis of the distribution data. The particle sizes were grouped according to standard U.S. Series sieve sizes as follows:

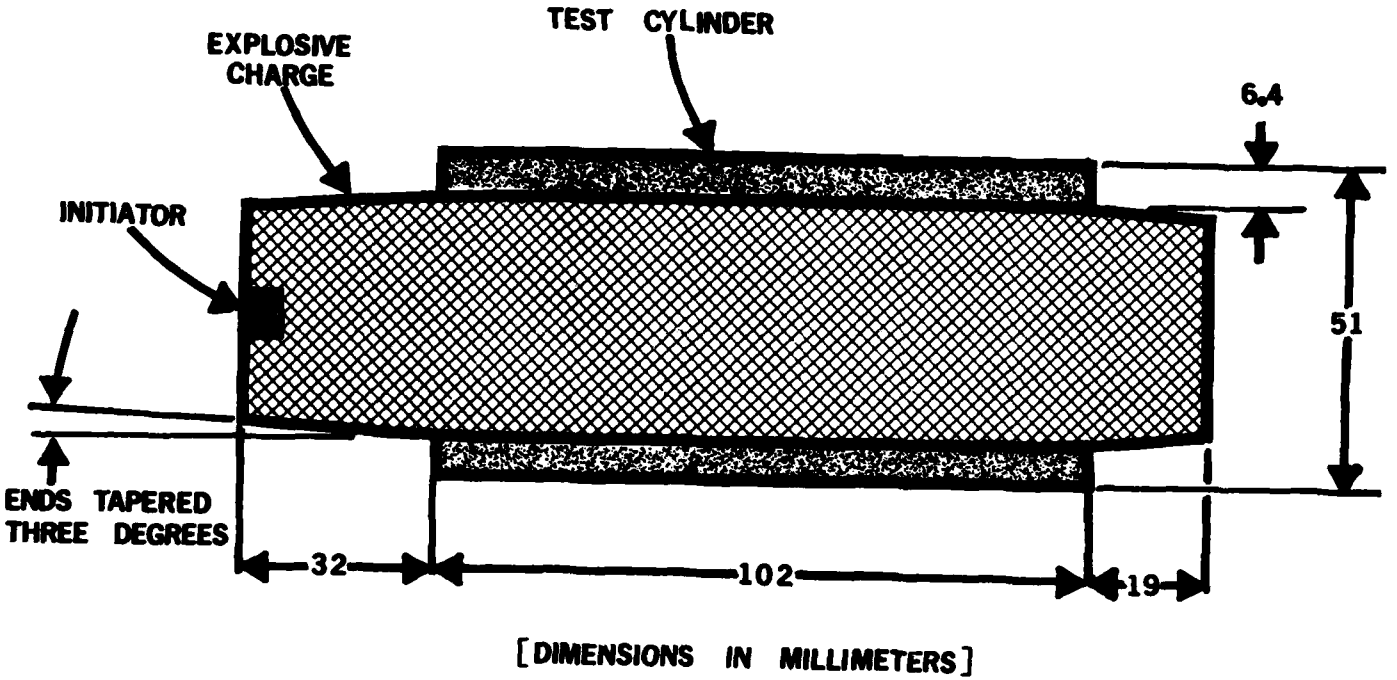

FIGURE 1. SPECIMEN GEOMETRY FOR EXPLOSIVE STRAIN RATE TESTS

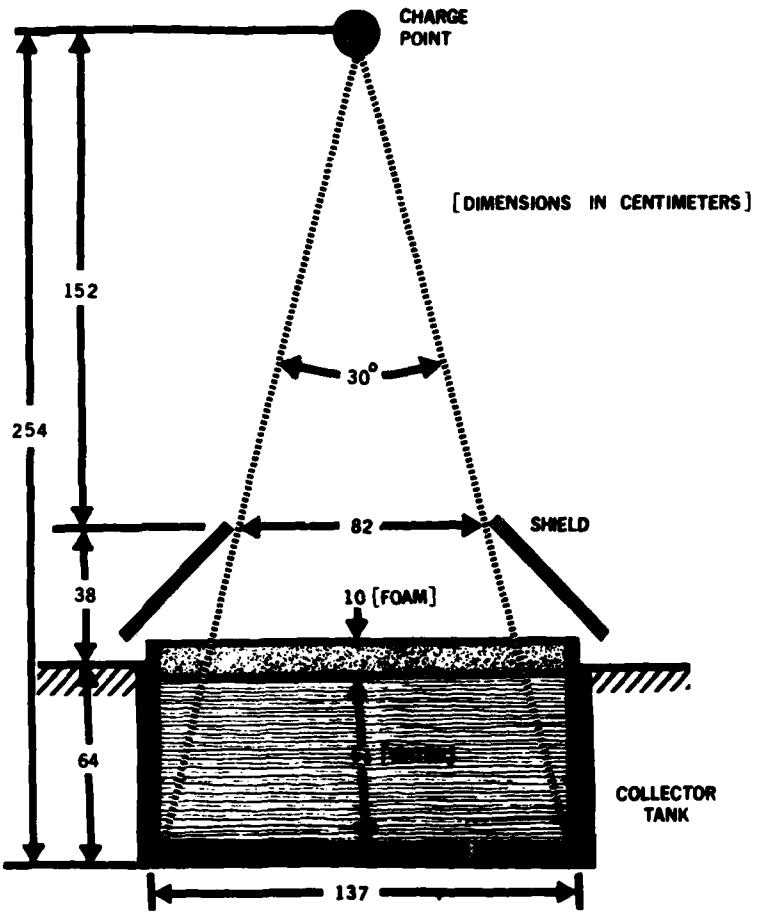

FIGURE 2. TEST SETUP FOR SOFT RECOVERY OF MATERIAL FROM EXPLOSIVE STRAIN RATE TESTS

Mesh Number	Opening (mm)
3	6.68
4	4.70
6	3.33
8	2.36
10	1.98
12	1.65
16	1.17

The particle size distributions obtained in triplicate tests on the seven material conditions are presented in Tables 3 and 4. These data have been corrected for efficiency of recovery and normalized to full-cylinder recovery, such that the average mass corresponding to any interval (sieve size) is identical to that calculated from the initial partial recovery data. The actual parameters that characterize the distribution are obtained from analysis of Mott plots of these data.

To construct a Mott plot, sieves are ordered from coarsest to finest mesh and the average mass of particles retained on each sieve is calculated. The logarithm of N_m, the cumulative number of fragments collected, is plotted as the ordinate and $\sqrt{m}$ is plotted as the abscissa. Because this distribution is highly skewed, any undue bias in assigning numbers to the data points produces highly misleading results. Such a bias results if we take N_m to be the total number of particles accumulated on a certain number of sieves because it positions a data point at the edge of an interval in a situation where the number of counting bins is quite limited. To correct this the number of particles assigned to the first sieve is taken to be half the number counted. This assumes the distribution is linear over small intervals, and half the particles will have mass less than the computed average mass for that sieve. Then half the particles on the next smaller sieve are added to all the particles on the larger sieve. This number is plotted as the average mass of the second sieve. This process is continued for all sieves and yields graphs such as presented in Figure 3, which also shows the particles recovered from a 30° sector of a typical shattered cylinder in relation to the size of the original cylinder. The lines through the data in the figures are the best straight lines fitted by linear regression to the function $N_m = N_o e^{-\sqrt{m}/\mu}$, the Mott distribution. Correlations to this function averaged 96% or better over the seven material conditions tested. The Mott number parameter, N_o, is simply the extrapolated intercept of these curves with the ordinate. The Mott size parameter, μ, is obtained as the square of the reciprocal slope of these curves. A summary of Mott parameters for all tests is presented in Table 5.

TABLE 3. FS-01 STEEL PARTICLE SIZE DISTRIBUTIONS

U.S. Sieve Size	Particle Count N_i	Total Mass M_i (g)	Particle Count N_i	Total Mass M_i (g)	Particle Count N_i	Total Mass M_i (g)
	Cylinder A-1		Cylinder A-2		Cylinder A-3	
3	0	0	0	0	0	0
4	108	62.8	89	64.6	129	76.8
6	1080	248.7	800	210.1	1010	243.0
8	1884	194.2	2074	208.6	1903	197.0
10	1260	60.1	1644	73.6	1722	83.7
12	1488	42.6	1852	50.1	1087	29.7
16	3540	49.4	4030	55.0	2485	33.1
	Cylinder B-1		Cylinder B-2		Cylinder B-3	
3	11	15.5	29	30.6	22	27.3
4	227	129.3	218	98.1	197	114.4
6	941	229.7	988	239.1	1064	265.1
8	1818	185.3	1874	197.2	1470	150.2
10	1082	50.9	1191	53.7	1272	55.7
12	952	26.7	886	25.8	899	24.7
16	2337	32.5	2208	28.3	2161	28.5
	Cylinder C-1		Cylinder C-2		Cylinder C-3	
3	0	0.0	26	38.3	29	38.3
4	236	156.8	261	152.5	315	208.0
6	1095	271.2	899	246.9	888	221.5
8	1519	159.5	1433	145.3	1232	139.8
10	930	45.6	808	39.1	687	33.0
12	577	15.8	1003	27.7	831	15.9
16	1743	23.2	2046	27.2	1389	21.5
	Cylinder D-1		Cylinder D-2		Cylinder D-3	
3	0	0	41	92.4	42	84.9
4	474	407.3	409	312.2	465	322.6
6	536	153.9	600	162.1	691	173.0
8	686	71.5	655	81.9	663	65.1
10	337	17.7	355	16.9	465	22.0
12	362	11.5	395	11.5	353	10.2
16	873	25.0	777	10.9	747	12.0

TABLE 4. HF-1 STEEL PARTICLE SIZE DISTRIBUTIONS

U.S. Sieve Size	Particle Count N_i	Total Mass M_i (g)	Particle Count N_i	Total Mass M_i (g)	Particle Count N_i	Total Mass M_i (g)
	Cylinder A-1		Cylinder A-2		Cylinder A-3	
3	0	0	0	0	0	0
4	136	76.3	157	67.7	179	91.2
6	829	232.3	964	228.2	930	225.6
8	1902	194.6	2024	212.7	2207	199.7
10	1399	70.9	1325	61.0	1551	69.6
12	1603	44.5	1518	42.0	1742	46.6
16	3818	50.1	3783	51.8	3555	47.9
	Cylinder B-1		Cylinder B-2		Cylinder B-3	
3	50	85.9	54	64.6	63	79.6
4	315	282.0	326	198.9	403	260.8
6	693	188.5	957	269.3	755	206.2
8	920	97.5	1120	120.1	1069	103.2
10	391	20.0	554	26.1	654	28.0
12	454	14.2	511	15.0	428	10.6
16	1009	14.2	674	9.8	755	9.9
	Cylinder C-1		Cylinder C-2		Cylinder C-3	
3	0	0	0	0	0	0
4	341	237.8	389	250.8	236	152.5
6	921	241.6	663	175.9	957	283.7
8	1401	136.9	1554	181.8	1586	147.4
10	681	30.5	834	40.4	1022	50.4
12	770	21.8	663	18.7	957	27.3
16	1842	24.0	1589	21.2	1795	25.4

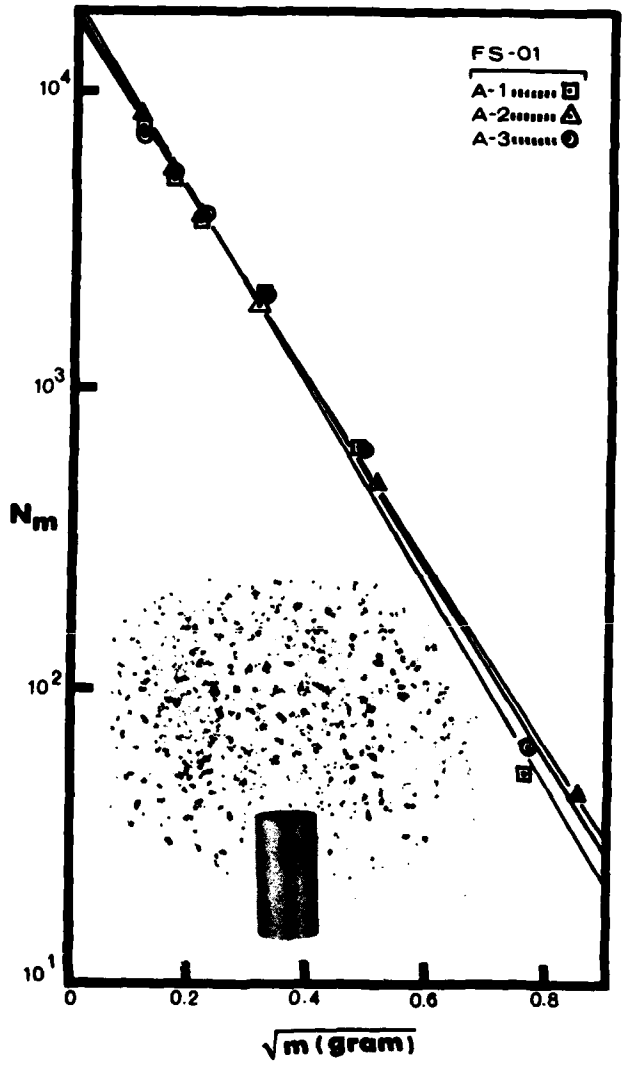

FIGURE 3. Mott Plots for FS-01 (A) Steel. N_m is the total number of particles having mass greater than m. Partial recovery data was normalized to full recovery. The particles recovered from a 30° sector of a typical cylinder are shown to provide a size perspective.

TABLE 5. MOTT PARAMETERS FOR EXPLOSIVE TESTS

Heat Treatment Designation	Test Cylinder Number	Initial Mass M_o (g)	Efficiency of Recovery	Mott Number Parameter N_o	Mott Size Parameter μ(mg)
FS-01 (A)	A-1	692	1.000	20265	17.4
	A-2	701	0.810	18011	20.1
	A-3	691	0.927	18453	19.4
FS-01 (B)	B-1	692	1.109	15256	23.1
	B-2	688	0.826	14647	23.8
	B-3	688	1.094	13562	25.5
FS-01 (C)	C-1	690	1.018	10623	34.1
	C-2	695	0.920	10615	33.2
	C-3	695	0.837	9610	34.9
FS-01 (D)	D-1	695	0.962	3999	104.9
	D-2	695	0.880	4002	98.3
	D-3	696	0.939	4474	88.9
HF-1 (A)	A-1	707	0.736	14958	25.3
	A-2	701	0.830	16528	22.8
	A-3	708	0.838	17578	21.8
HF-1 (B)	B-1	710	0.793	5460	65.5
	B-2	709	0.920	5995	75.8
	B-3	707	0.795	5771	70.9
HF-1 (C)	C-1	708	0.792	8290	46.7
	C-2	706	0.875	8565	44.8
	C-3	705	0.763	9953	35.0

Crack Branching Studies: After completing the characterization of the materials in terms of both mechanical properties and particle size distributions, the crack branching stress intensity factors for each material were determined. Although it is rather easy to induce crack branching in a brittle material, the analysis used to calculate the stress intensity factor at branching in all but the simplest geometries is often suspect. The dynamics of fracture in finite specimens is not well described; most of the analyses are for infinite specimens or physically artificial cracks. One is forced to construct an operational definition of the crack branching stress intensity factor for finite specimen geometry. The most practical approach to inducing branch cracks in a metal is to load a blunt notched specimen in tension. Unfortunately, acceleration of the resulting crack is far more intense than would be experienced by a sharp natural crack, and the average strain energy density in the material is considerably higher. Changing the notch stress concentration factor changes the fracture load but presumably not the crack branching stress intensity factor.

The specimen developed for these studies is a modified single-edge-notch (SEN) tension specimen with a blunt notch of constant root radius equal to 1.27 mm. This specimen and the formulation of the static stress intensity factor for arbitrary crack length are illustrated in Figure 4.

The high hardness of the materials being investigated creates a need for special gripping arrangements to load a plate in tension. Anthony (4) solved this by bonding soft mild steel plates to the specimen grip areas with an epoxy resin. The approach in the current work has been to use pin-loading, reducing the gage section sufficiently for large fracture loads to be applied without fracturing the specimen at the pin holes. The length of the reduced section, i.e., the gage length, was 20 cm and the separation of load points was 30 cm. This assures that the tensile field in the 5 cm wide notch region is unperturbed by the presence of the loading pins.

The fracture stress, and therefore the average strain energy density, was controlled by varying the depth (a_o) of the constant radius notch root. When a crack erupts from the notch root, it is subjected to higher strain energies than would be expected for a sharp crack initiating under a similar loading geometry. The situation may be viewed as an instantaneous elevation of the stress field intensity. It is assumed that the apparent stress intensity factor for this initial crack is reasonably described by the stress intensity factor characteristic of a sharp crack having length equal to the notch depth, but the situation is clearly dynamic and requires calculation of an appropriately corrected stress intensity factor as given by:

$$K_{dynamic}\,(a,v,\sigma) = \{K_{static}\,(a,\sigma)\}\{f(v)\} \qquad (2)$$

where $K_{static}\,(a,\sigma)$ is the static stress intensity factor calculated for

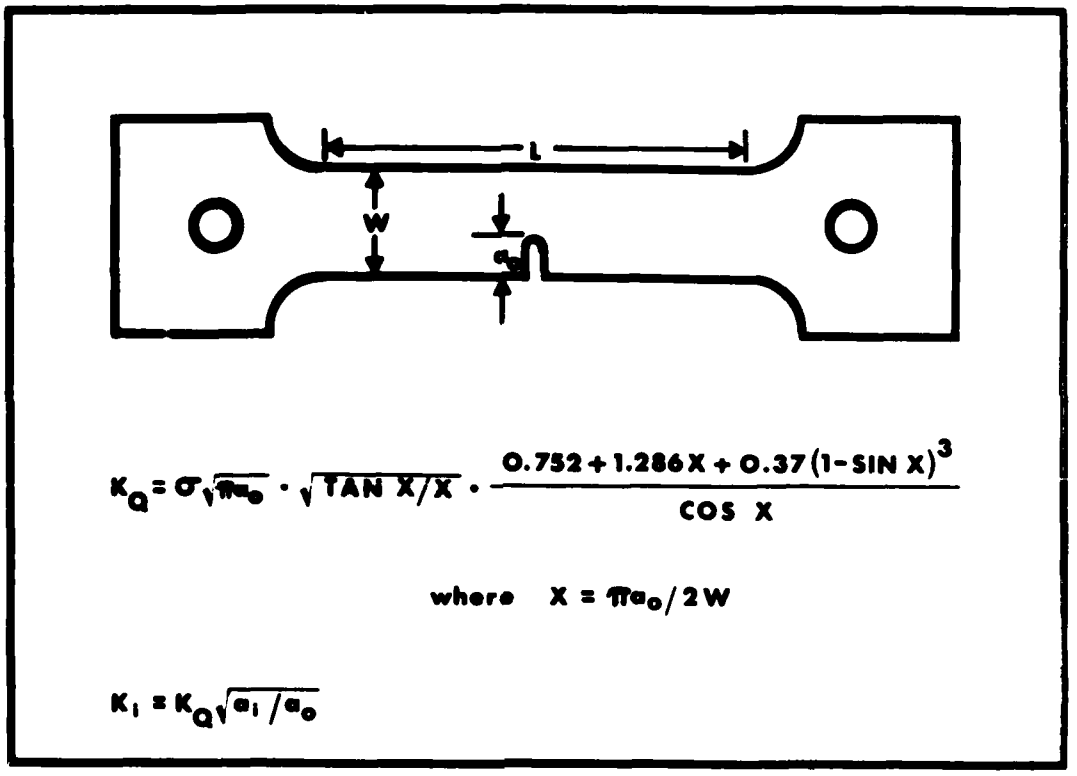

FIGURE 4. Modified Single-Edge-Notch Tension Specimen Used to Investigate Crack Branching. The length-to-width ratio (L/W) in the gage section was greater than 4, and strain energy density was varied by changing the notch depth (a_o).

a crack length, a, in a particular specimen geometry loaded by stress, σ. The factor f(v) is the dynamic correction to the stress intensity factor necessitated by the effects of material inertia. According to published works on elastodynamic cracks, f(v) is a function only of crack velocity.

To calculate the static stress intensity factor for a sharp crack that has catastrophically initiated from a blunt notch, assume that this stress intensity factor takes the following form

$$K_{static}\ (a_i,\sigma) \equiv \{K_Q\ (a_o,\sigma)\}\ \{g(a_i,a_o)\} \qquad (3)$$

where K_Q is the apparent stress intensity factor at initial fracture and g is a correction factor to accommodate extended cracks, a_i is the instantaneous crack length, a_o is the starting crack length (notch depth), and σ is the fracture stress.

Among the solutions for crack tip stress fields, that of Tada, Paris, and Irwin [10] appears to be the most precise expression for stress intensity factor in the single-edge-notch tension specimen. His result is

$$K_Q = \sigma\sqrt{\pi a_o}\ .\ \sqrt{(\tan X)/X}\ .\ \frac{0.752 + 1.286X + (0.37)\ (1 - \sin X)^3}{\cos X} \qquad (4)$$

where $X = \pi a_o/2W$

and σ is applied stress; a_o is initial crack length or, for present purposes, notch depth; W is specimen width.

This expression must be modified to represent reasonably the change in static stress intensity factor that occurs when the crack length increases from a_o to a_i. Because the specimen geometry was designed with particular attention to eliminating the possibility of stress wave reflections from the boundaries during short, rapid crack runs, it is reasonable to seek a first correction to the solution which describes the crack as if it had statically extended in an infinite medium. The simplest possibility is the Griffith crack, for which the stress intensity factor increases as the square root of the crack length. For such a flaw the stress intensity factors for cracks of different lengths have the ratio

$$\frac{K_i}{K_o} = \sqrt{\frac{a_i}{a_o}} \qquad (5)$$

Neglecting dynamic corrections for the moment, the case of rapid incremental extension of a crack in the SEN specimen is analogous to extension of a Griffith flaw in an infinite specimen for purposes of calculating static stress intensity factors. Therefore, equation (5) is adopted as the correction factor necessary to calculate the static

stress intensity factor for instantaneous crack length, a_i, from Tada's expression for K_Q {equation (4)}. Specifically,

$$g\ (a_i,\ a_o) \equiv \sqrt{\frac{a_i}{a_o}} \tag{6}$$

The velocity correction used in this work assumes the crack is traveling at 40% of the Rayleigh wave velocity (C_R), which is assumed to be the limiting velocity. This is based on several considerations, the first of which is the experimental work of Schardin (11), who demonstrated with high speed photography that the speed of advance of the locus of crack fronts in a process of fracture by multiple branching was on the order of 95% of the terminal velocity for individual cracks in glass specimens. He also shows that increasing the applied tension decreases the distance to initiate a branch point. This inverse relationship between stress and crack length is suggestive of the stress intensity factor and qualitatively supports the notion that $K_B \sim \sigma\ (\pi a_B)^{1/2}$ for an infinite plate may be a material constant. The observation on terminal velocity implies that the crack spends very little of its travel time undergoing intense acceleration and thus limiting velocity is approached in a very short distance. Further support for this view is provided by Kerkhof (12), who used ultrasonic fractography to measure crack velocity in glass. By introducing ultrasonic waves into a tensile fracture specimen, the maximum principal stresses that govern the direction of crack propagation are made to vary periodically in space and time. As a consequence the fracture surface topography exhibits waviness, and the wavelength is determined by the ratio of the crack speed to the frequency of the ultrasonic modulator. Very precise local determinations of crack speed are possible using simple optical microscopy and appropriate lighting. Kerkhof observed that the crack speed was approximately constant through most of the mirror zone and was, in fact, the terminal velocity at the point where deep surface hackle (microbranching) began. He also discusses why surface measurements of the trace velocity of non-uniformly propagating cracks can lead to questionable results. A variety of common techniques for measuring crack speeds has been described elsewhere (13). It is sufficient to note that no presently available technique for measuring crack speeds in metals has the resolution to permit conclusive statements about the crack speed and acceleration in the pseudo- mirror zone of brittle metals to be made. It is here that attention needs to be focused. Consequently, it is reasonable to assume, by analogy to Kerkhof's work, that the best estimate of crack speed at incipient bifurcation is locally equal to the terminal velocity in brittle steel ($0.4\ C_R$).

The numerical value assigned to f(v) in equation (2) depends upon which crack model is used. Sih and Irwin (14) consider the problem of evenly spaced radial cracks originating at a point and terminating on a circular locus to estimate dynamic crack-extension force (G). The correction factor depends upon both crack speed and Poisson's ratio and

is approximately 0.77 for the conditions assumed to prevail in the present work. The analysis of Freund (15) is based upon a single dynamic crack and implies that 0.72 is the correction factor. These are obviously equivalent, but because the cracks considered here require analysis from initiation to branching, they fall more naturally under Freund's analysis. The final expression adopted for calculating dynamic stress intensity factors in the single-edge-notch tension specimen may now be written as

$$K_{dynamic}\ (a_i, a_o, \sigma, v) = 0.72\ \sqrt{a_i/a_o}\ K_Q\ (a_o, \sigma) \qquad (7)$$

where a_i is the instantaneous length of the dynamic crack, a_o is the starting notch depth, and K_Q is the apparent stress intensity factor given by equation (4).

Using this formulation of the dynamic stress intensity factor, it is possible to estimate the strain energy release rates associated with significant features detected on the fracture surface during post-mortem analysis of failed specimens.

Specimens were machined to the geometry shown in Figure 4 and heat-treated to the conditions listed in Table 1. Crack branching tests were performed by loading the specimens to failure in uniaxial tension on a universal materials testing machine. These tests were conducted at room temperature in a displacement control mode to provide maximum stiffness in the load train. Quasistatic displacements were used in order to assume "fixed-grip" conditions in the analysis. This means that fracture energies come only from the high strain energy densities stored in the specimens themselves and not from any cross-head motion in the testing machine. The test series for each material condition consisted of a range of notch depths selected to provide a range of fracture stresses.

A typical example of a full branch profile is shown in Figure 5. Such samples were prepared by removing unwanted material outside the crack branching zone with an abrasive cut-off wheel and reconstructing the specimen from recovered fragments. The assemblage was then fixed in Kold-Mount and a belt sander was used to remove half the specimen thickness. Specimens were then metallographically polished and etched; the view in the photograph is a fracture profile along the vertical mid-plane of the specimen. Macroscopic branch cracks were found which exhibited all the behavior patterns alluded to by Irwin (16). In general, the micro-branch planes were oriented at angles of 20-40° to the primary crack plane.

Examination of the fracture surfaces of brittle metals revealed three clear features that are analogous to features found on glass fracture surfaces (Figure 6). These are a pseudo-mirror region containing the fracture origin centered at a distance a_M from the specimen

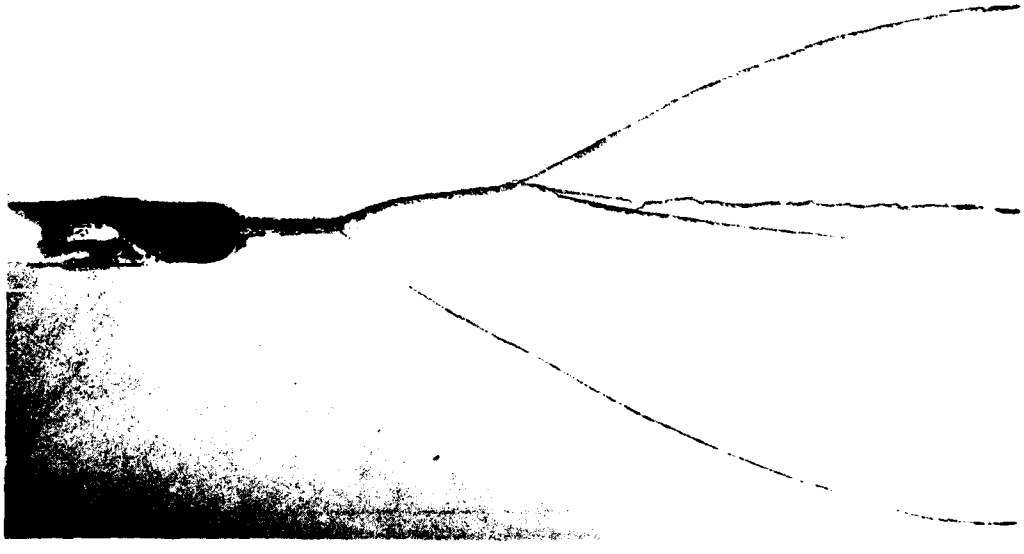

FIGURE 5. Crack Branching Profile on Mid-Plane of FS-01 (B) Steel Specimen (2.5 X). Note the skewing and subsequent arrest of the main crack.

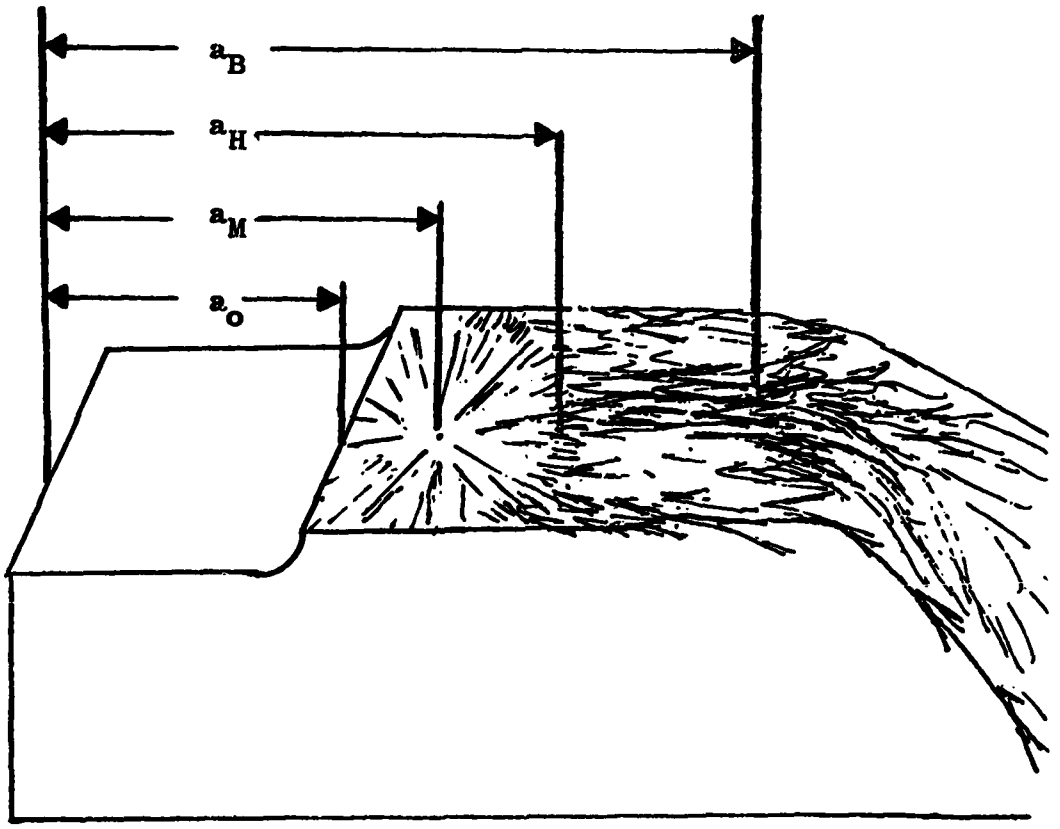

FIGURE 6. Macroscopic features of branching crack surface in a brittle metallic SEN specimen. Notch depth is a_o; distance to fracture origin is a_M; crack length at incipient branching (hackle) is a_H; and crack length at full bifurcation is a_B.

edge, a definable boundary to that region beyond which deep hackle occurs, a_H, and a point where the primary fracture fully bifurcates, a_B. Hackle and incipient microbranching are considered to be the same. Because the boundary separating that region from the mirror zone is approximately semi-circular, a_H was defined to be the deepest penetration of that boundary from the specimen edge at which the fracture initiated. The detailed results of the crack branching tests for all materials are presented in Tables 6 through 12. It can be seen that full bifurcation did not always occur even in the most brittle conditions. Examination of the data for materials that had both branched and unbranched fractures indicates that insufficient fracture stress (or strain energy) is not the explanation. It was observed both here and in the work of Anthony (4) that full branching is the culmination of a build-up of microbranch trials until one of these microbranches can develop into an independent crack. Thus there appears to be a statistical quality about the full branch crack even when the crack extension forces are adequate.

Because hackle always occurred, it was adopted as a more convenient property than macrobranching. The dynamic stress intensity factors for hackle (K_H) and branching (K_B) are independent of notch depth and fracture stress in all material conditions. This fact is clearly illustrated by Figures 7 through 10, in which the dotted horizontal lines are the calculated mean values of K_H and K_B. Such independence lends further credence to the interpretation of K_H and K_B as material properties.

SEM Fractography of High Energy Fractures

Numerous fracture surfaces from tensile tests, plane strain fracture toughness tests, crack branching tests, and explosive fragmentation tests were examined by scanning electron microscopy. Typical results are illustrated and discussed for each material. All four conditions of FS-01 steel produced fractures that were essentially the same fractographically, regardless of the type of test specimen and, therefore, the magnitude of the strain rate causing specimen failure. Figure 11 shows the basic features of fracture surfaces of FS-01 (C) steel. This material is a high quality tool steel with a characteristically broad dispersion of fine carbides that serve as nuclei for void growth. The general fracture mode seems to be void-nucleated quasi-cleavage. It is clear from the figures that the fracture mechanism is the same for crack branching and explosive loading test specimens.

Fractographs of HF-1 (A) steel are shown in Figure 12. Again the fractures are identical in the crack branching and explosive loading tests; the fracture is clearly intergranular. The fracture surfaces of HF-1 (B) steel are shown in Figure 13. A high velocity fracture surface near a branch point from a SEN test specimen is shown in Figure 13A; the fracture is intergranular. The explosive test produced the surface shown in Figure 13B, which shows additional features. The

TABLE 6. FS-01 (A) CRACK BRANCHING TEST RESULTS

		Crack Lengths (mm)				Stress Intensity Factors (MPa$\sqrt{m}$)		
Specimen Number	Fracture Stress σ_F(MPa)	Original Notch a_o	Fracture Origin a_M	First Hackle a_H	First Branch a_B	Initial (Apparent) K_Q	at Hackle K_H	at Branch K_B
1	544.5	6.60	6.76	11.76	22.23	96.9	93.1	128.0
2	626.0	4.12	4.57	9.40	16.69	83.6	91.0	121.2
3	679.8	2.41	2.95	6.91	-	67.8	82.6	-
4	596.8	5.08	5.56	11.13	15.70	90.1	96.0	114.1
5	454.7	6.40	6.99	13.18	25.32	79.4	82.0	113.7
6	443.2	8.08	8.10	16.97	-	90.7	94.6	-
7	469.9	9.14	9.47	14.38		105.5	95.2	-
8	641.2	3.73	4.06	8.53	16.08	81.0	88.2	121.1
9	526.3	5.39	5.41	11.91	22.12	82.3	88.2	120.1
10	667.6	6.48	6.71	8.84	11.20	117.4	98.8	111.2
11	567.9	7.87	8.26	10.26	14.00	114.1	93.8	109.6
12	514.9	9.09	9.63	12.14	22.76	115.0	95.7	131.0

TABLE 7. FS-01 (B) CRACK BRANCHING TEST RESULTS

Specimen Number	Fracture Stress σ_F(MPa)	Crack Lengths (mm)				Stress Intensity Factors (MPa$\sqrt{m}$)		
		Original Notch a_o	Fracture Origin a_M	First Hackle a_H	First Branch a_B	Initial (Apparent) K_Q	at Hackle K_H	at Branch K_B
1	905.0	3.43	4.65	5.26	6.48	109.3	97.4	108.1
2	911.1	4.65	5.82	6.40	8.92	130.8	110.5	130.4
3	584.4	5.74	5.97	8.10	30.40	95.4	81.6	158.1
4	899.7	6.22	7.52	8.89	9.63	154.6	133.1	138.5
5	557.6	7.85	9.07	10.16	25.02	112.3	92.0	144.3
6	527.9	9.91	10.67	12.14	15.55	127.2	101.4	114.7
7	600.0	12.73	13.49	13.89	16.69	179.3	134.9	147.8
8	853.2	8.89	9.35	9.68	18.64	187.3	140.7	195.2
9	564.4	14.00	14.25	14.64	17.17	185.8	136.8	148.2
10	565.2	11.46	12.07	12.52	15.16	152.8	115.1	126.6

TABLE 8. FS-01 (C) CRACK BRANCHING TEST RESULTS

Specimen Number	Fracture Stress σ_F(MPa)	Crack Lengths (mm)				Stress Intensity Factors (MPa$\sqrt{m}$)		
		Original Notch a_o	Fracture Origin a_M	First Hackle a_H	First Branch a_B	Initial (Apparent) K_Q	at Hackle K_H	at Branch K_B
1	588.2	13.97	14.25	17.30	-	193.3	154.8	-
2	819.0	8.74	9.53	11.58	23.19	177.4	147.1	208.1
3	489.4	10.24	10.69	17.96	-	120.2	114.6	-
4	983.5	7.93	7.95	9.25	16.66	198.4	154.3	207.1
5	748.8	12.62	13.77	15.70	-	221.9	178.2	-
6	886.6	11.68	12.19	13.21	-	238.6	182.6	-
7	887.6	6.71	6.99	11.56	17.98	159.6	150.9	188.2
8	579.8	15.24	15.55	16.89	-	209.7	158.9	-
9	1185.9	5.21	5.87	9.17	19.13	181.8	173.7	250.8
10	1284.9	4.57	4.60	6.02	13.61	182.3	150.6	226.5

TABLE 9. FS-01 (D) CRACK BRANCHING TEST RESULTS

Specimen Number	Fracture Stress σ_F(MPa)	Crack Lengths (mm)				Stress Intensity Factors (MPa$\sqrt{m}$)		
		Original Notch a_o	Fracture Origin a_M	First Hackle a_H	First Branch a_B	Initial (Apparent) K_Q	at Hackle K_H	at Branch K_B
1	1185.3	6.30	7.47	10.77	-	204.7	192.7	-
2	988.9	8.94	9.85	13.03	-	218.1	189.6	-
3	1186.8	7.80	8.53	9.73	-	236.5	190.2	-
4	667.1	15.37	15.90	17.68	-	243.9	188.3	-
5	864.3	12.73	13.59	15.19	-	258.0	203.0	-
6	895.3	10.44	11.43	13.54	-	223.5	183.3	-
7	689.6	14.10	14.61	15.67	-	228.7	173.6	-
8	916.4	11.66	12.32	14.53	-	252.0	202.5	-

TABLE 10. HF-1 (A) CRACK BRANCHING TEST RESULTS

Specimen Number	Fracture Stress σ_F(MPa)	Crack Lengths (mm)				Stress Intensity Factors (MPa$\sqrt{m}$)		
		Original Notch a_o	Fracture Origin a_M	First Hackle a_H	First Branch a_B	Initial (Apparent) K_Q	at Hackle K_H	at Branch K_B
1	267.3	12.75	14.48	16.87	-	80.2	66.4	-
2	321.5	11.58	12.50	17.60	-	88.0	78.1	-
3	441.6	7.67	9.27	13.97	-	87.3	84.8	-
4	368.3	10.31	12.50	16.18	-	90.9	82.0	-
5	340.7	10.16	11.91	15.93	-	83.2	75.0	-
6	499.7	6.68	9.55	12.22	17.58	89.7	87.4	104.8
7	382.9	8.92	10.57	13.51	-	84.3	74.8	-
8	371.6	8.79	10.97	15.14	-	81.0	76.6	-
9	430.7	7.11	8.94	12.83	-	80.7	78.0	-
10	476.3	6.22	8.41	13.59	-	81.7	86.9	-

TABLE 11. HF-1 (B) CRACK BRANCHING TEST RESULTS

Specimen Number	Fracture Stress σ_F (MPa)	Crack Lengths (mm)				Stress Intensity Factors (MPa$\sqrt{m}$)		
		Original Notch a_o	Fracture Origin a_M	First Hackle a_H	First Branch a_B	Initial Apparent K_Q	at Hackle K_H	at Branch K_B
1	565.8	10.47	11.56	15.04	-	141.4	122.1	-
2	539.9	10.64	12.09	16.71	-	136.8	123.5	-
3	519.1	12.17	13.21	17.96	-	148.4	129.8	-
4	471.9	12.98	14.61	16.56	22.23	143.5	116.7	135.2
5	460.4	13.31	14.17	17.04	24.00	143.7	117.1	138.9
6	546.5	12.12	12.95	16.05	-	155.7	129.0	-
7	592.5	10.11	11.61	14.83	21.41	143.8	125.4	150.7
8	603.4	10.69	11.94	14.66	-	153.6	129.5	-

TABLE 12. HF-1 (C) CRACK BRANCHING TEST RESULTS

Specimen Number	Fracture Stress σ_F (MPa)	Crack Lengths (mm)				Stress Intensity Factors (MPa$\sqrt{m}$)		
		Original Notch a_o	Fracture Origin a_M	First Hackle a_H	First Branch a_B	Initial Apparent K_Q	at Hackle K_H	at Branch K_B
1	607.7	9.04	11.68	12.32	-	135.7	114.0	-
2	503.2	8.94	11.89	14.38	-	111.0	101.4	-
3	483.7	9.14	10.95	13.87	-	108.5	96.2	-
4	638.4	9.20	11.48	11.84	-	144.0	117.6	-
5	688.1	6.35	9.02	11.96	-	119.6	118.2	-
6	673.1	6.83	8.56	11.51	-	122.6	114.6	-
7	560.7	7.75	9.47	10.87	-	111.4	95.0	-
8	676.9	8.31	10.34	12.55	-	141.5	125.2	-

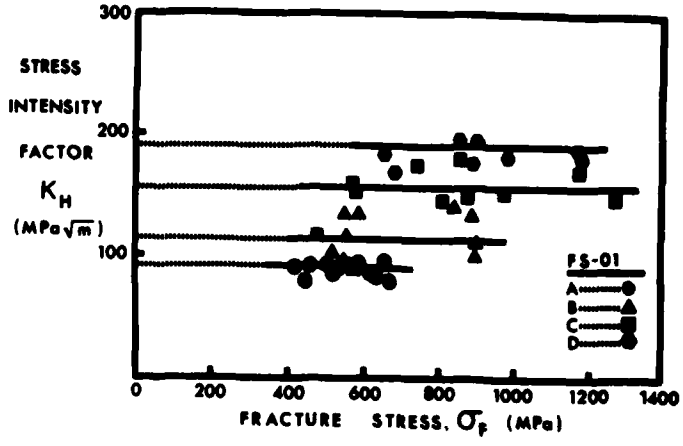

FIGURE 7. Dynamic Stress Intensity Factors for Hackle Versus Fracture Stress for All Conditions of FS-01 Steel.

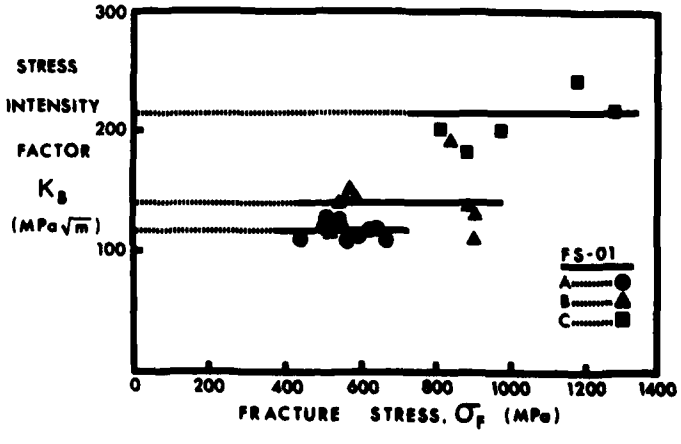

FIGURE 8. Dynamic Stress Intensity Factors for Crack Branching Versus Fracture Stress for All Conditions of FS-01 Steel.

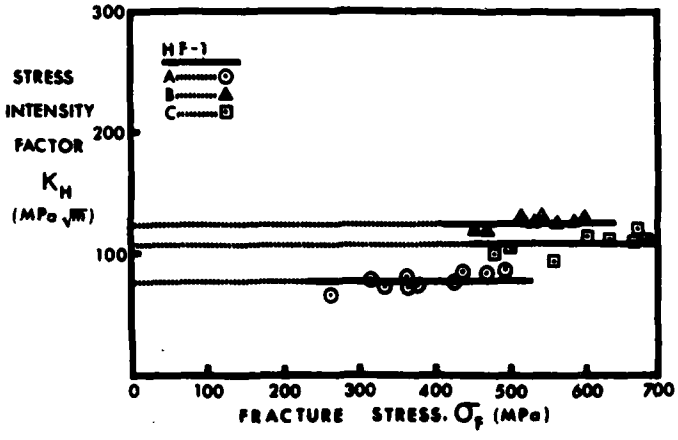

FIGURE 9. Dynamic Stress Intensity Factors for Hackle Versus Fracture Stress for All Conditions of HF-1 Steel.

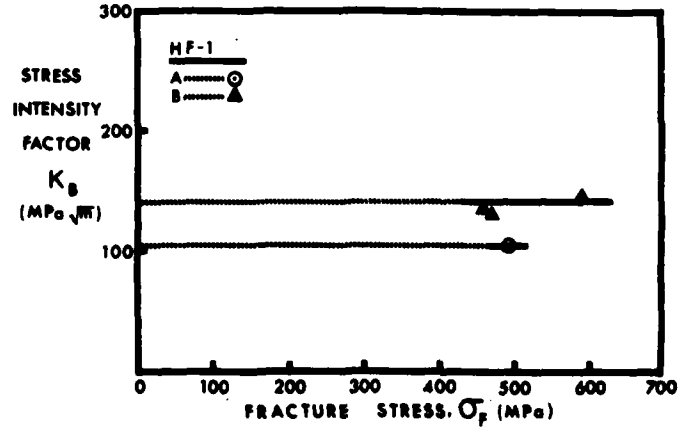

FIGURE 10. Dynamic Stress Intensity Factors for Crack Branching Versus Fracture Stress for All Conditions of HF-1 Steel.

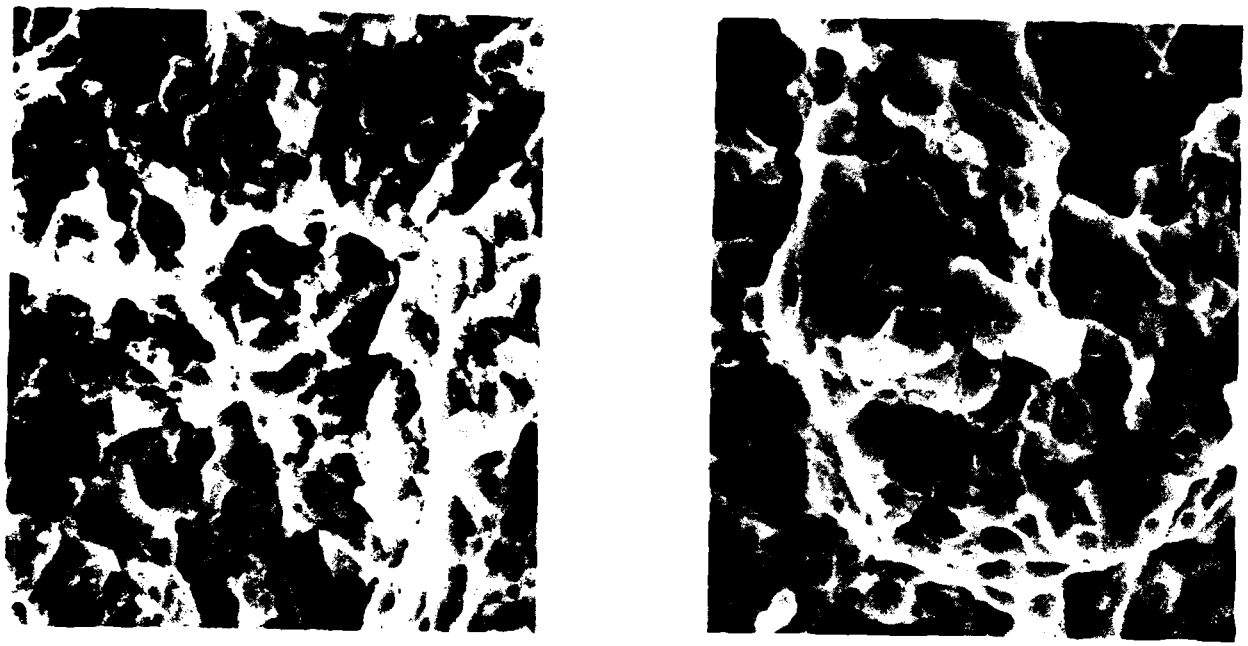

A. Vicinity of a microbranch crack near point of full bifurcation of main crack in SEN fracture specimen (3000X).

B. Vicinity of a microbranch crack on radial fracture surface of particle recovered from explosive test (3000X).

Figure 11. SEM Fractographs of FS-01 (C) Steel Samples. Cracks Propagated from Left to Right.

A. Vicinity of a microbranch crack near point of full bifurcation of main crack in SEN fracture specimen (125 X).

B. Vicinity of a microbranch crack on radial fracture surface of particle recovered from explosive test (125 X).

Figure 12. SEM Fractographs of HF-1 (A) Steel Samples. Cracks Propagated from Left to Right.

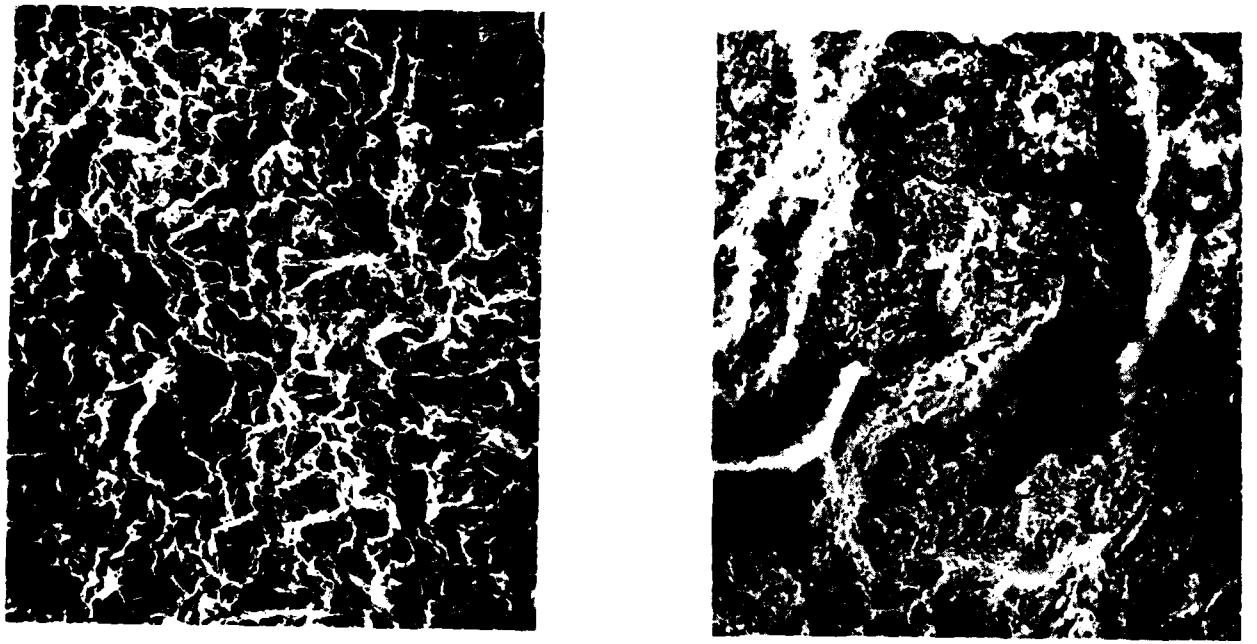

A. Vicinity of a microbranch crack near point of full bifurcation of main crack in SEN fracture specimen (125 X).

B. Vicinity of a microbranch crack on radial fracture surface of particle recovered from explosive test (125 X).

Figure 13. SEM Fractographs of HF-1 (B) Steel Samples. Cracks Propagated from Left to Right.

surface has been somewhat damaged by abrasion and oxidation (white fringes). There are, however, undamaged regions that show the same intergranular fracture as the branching specimen. The most striking feature is the presence of shear bands which are the thin vertical lines in the upper right hand side of the photograph. What is significant is that the microbranch cuts through these bands which are in approximate alignment across the crack opening. This indicates that the bands were there first and the brittle radial cracks followed. Figure 14 illustrates the intergranular nature of the fracture in HF-1 (C) steel. In spite of the surface damage to the particle recovered from an explosive test, the primary fracture shows a strong intergranular component. The extent of grain growth in the HF-1 (A) and HF-1 (C) heat treatments is also evident by comparison with HF-1 (B), which had little or no grain growth because of the moderate austenitizing temperature.

DISCUSSION OF EXPERIMENTAL RESULTS AND COMPARISON WITH THEORY

The numerical results of the previous sections have been evaluated in terms of mean values for each material and heat treatment. Standard deviations have also been computed. Those properties relevant to the proposed model are: plane strain fracture toughness (K_{IC}), dynamic stress intensity factors for hackle (K_H) and microbranching (K_B), and the Mott statistical parameters for number (N_o) and size (μ). A complete listing is provided in Table 13. Calculations indicated that a fourth power relationship should exist between the Mott number and size parameters and the K_B/K_{IC} ratio. Subsequent experimental results indicated that K_H/K_{IC} would be more appropriate than K_B/K_{IC}. The phenomenology of crack branching itself provides a rationale for this behavior. Prior to full bifurcation, the microbranch trials produce progressively longer cracks, the lengths of which are greater than average fragment dimensions. It is for this reason that K_H was considered to be not merely more convenient but perhaps more significant than K_B in the explosive strain rate regime in which brittle metals actually shatter. However, it is reasonable that the crack extension force, G_B, for a bifurcated crack (i.e., two cracks) should be about twice the extension force, G_H, for a single dynamic crack about to attempt branching. The observed ratio G_B/G_H was found to be 1.7 ($\pm$0.5) over all material conditions. The approximate proportionality of K_H to K_B further justifies the use of the more convenient experimental property, namely K_H. Figures 15 and 16 are log-log plots of the Mott size parameter, μ, as a function of the K_H/K_{IC} ratio and the Mott number parameter, N_o, as a function of the K_H/K_{IC} ratio. The best straight line fitted by linear regression through the HF-1 data yielded the following results:

$$\mu^H = 1.10\ (K_H/K_{IC})^{3.52}\ \text{milligrams} \qquad (8)$$

$$N_o^H = 2.82 \times 10^5\ (K_H/K_{IC})^{-3.30} \qquad (9)$$

A. Vicinity of a microbranch crack in SEN fracture specimen (125 X).

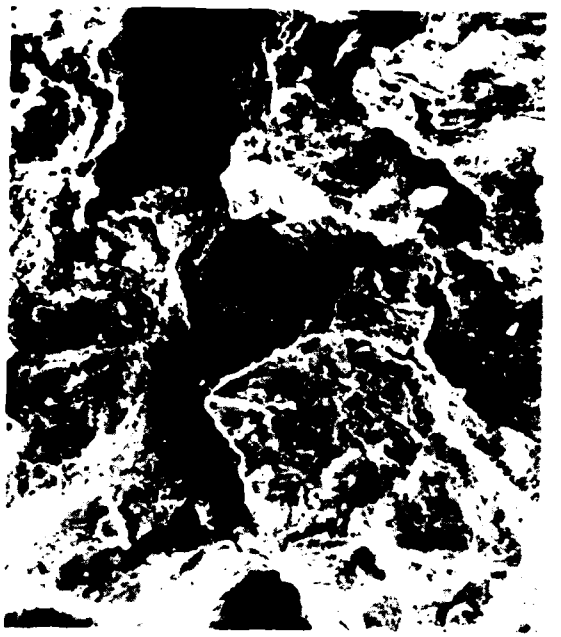

B. Vicinity of a microbranch crack on radial fracture surface of particle recovered from explosive test (125 X).

Figure 14. SEM Fractographs of HF-1 (C) Steel Samples. Cracks Propagated from Left to Right.

TABLE 13. SUMMARY OF CRACK BRANCHING AND EXPLOSIVE TESTING RESULTS[a]

Heat Treatment Designation	Plane-Strain Fracture Toughness K_{IC} (MPa$\sqrt{m}$)	Stress Intensity Factor at Hackle K_H (MPa$\sqrt{m}$)	Stress Intensity Factor at Full Branching K_B (MPa$\sqrt{m}$)	Mott Number Parameter N_o	Mott Size Parameter μ (mg)
FS-01 (A)	21.7 (±0.5)	91.6 (± 5.3)	118.9 (± 7.4)	18910 (±1190)	19.0 (±1.4)
FS-01 (B)	24.4 (±2.1)	114.4 (±21.1)	141.2 (±24.6)	14490 (± 860)	24.1 (±1.2)
FS-01 (C)	31.4 (±1.8)	156.6 (±19.4)	216.1 (±23.6)	10280 (± 580)	34.1 (±0.9)
FS-01 (D)	57.3 (±5.8)	190.4 (± 9.6)	(b)	4160 (± 270)	97.4 (±8.0)
HF-1 (A)	32.5 (±1.0)	79.0 (± 6.5)	104.8	16360 (±1320)	23.3 (±1.8)
HF-1 (B)	37.5 (±4.0)	124.1 (± 5.3)	141.6 (± 8.1)	5740 (± 270)	70.7 (±5.2)
HF-1 (C)	40.3 (±3.3)	110.3 (±11.3)	(b)	8940 (± 890)	42.2 (±6.3)

(a) Results stated as the mean value (± one standard deviation).

(b) Full branching of cracks not observed in these material conditions.

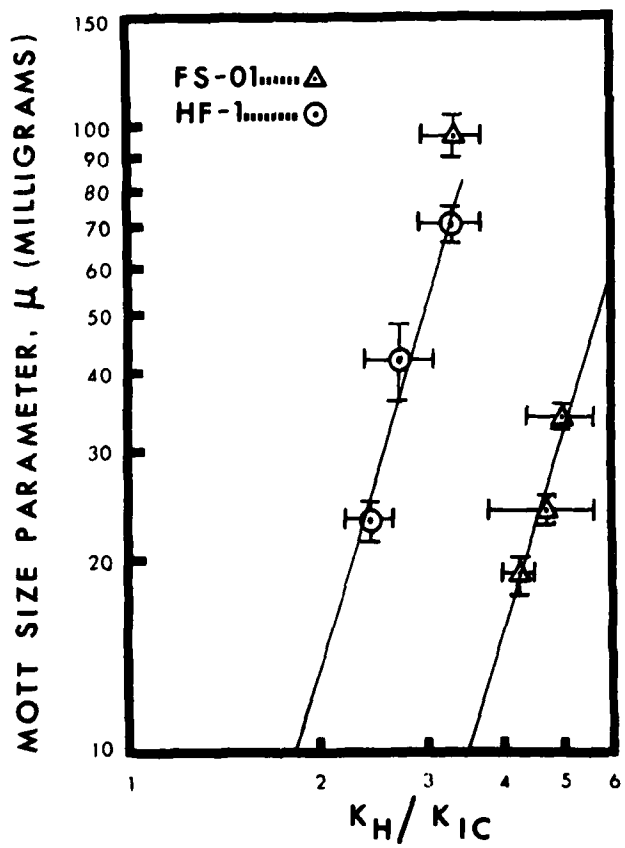

FIGURE 15. Mott Size Parameter, μ, as a Function of the K_H/K_{IC} Ratio.

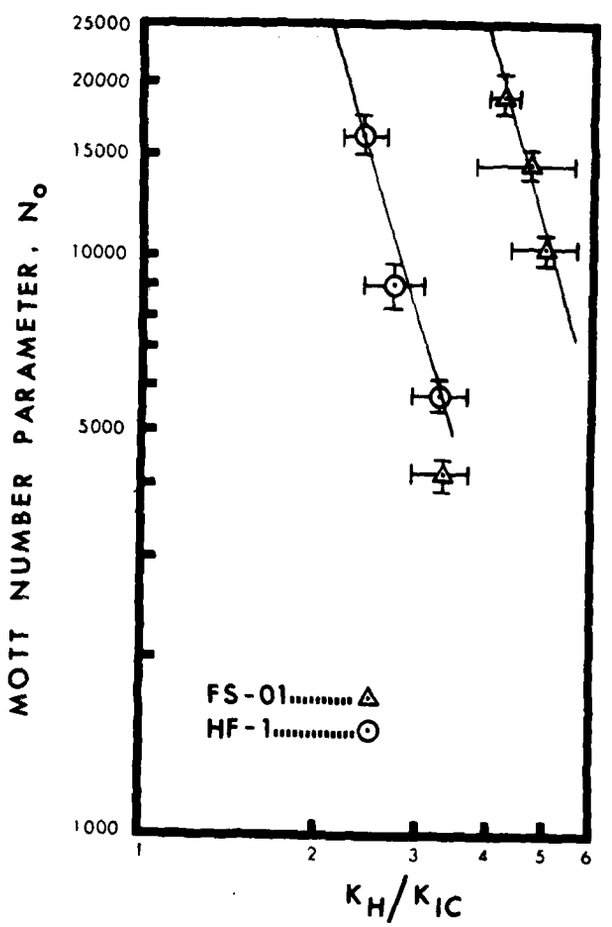

FIGURE 16. Mott Number Parameter, N_0, as a Function of the K_H/K_{IC} Ratio.

The best straight line fitted by linear regression through the three lowest-mass points in the FS-01 data yielded the following results:

$$\mu^F = 0.14\ (K_H/K_{IC})^{3.37}\ \text{milligrams} \tag{10}$$

$$N_o^F = 3.16 \times 10^6\ (K_H/K_{IC})^{-3.54} \tag{11}$$

The exponents in equations (8) through (11) relating the Mott parameters μ and N_o to the K_H/K_{IC} ratio for both materials are equal within experimental uncertainties. The average value of 3.43 ($\pm$0.12) compares favorably with the model prediction of 4. The FS-01 ($\bar{D}$) data were omitted from the calculations because they would obviously have distorted the results. The omission is justified on several grounds. The tests barely met the plane strain criterion, i.e., fracture specimens had sizable shear lips; moreover the particles recovered from the explosive tests were predominantly bounded by shear surfaces and therefore not suited to the opening mode analysis used in this work. That particular datum is useful in that it sets definite bounds on the model developed here, which apparently works only for shatter of brittle cylinders exhibiting substantial radial components of fracture.

A final comment is in order regarding the nature of the crack velocity correction. Both experimental limitations and analytical considerations led to applying the same correction factor to all static K_H and K_B calculations. The finally determined functional relationships are simply power laws. Omission of this velocity correction, i.e., using the static values of stress intensity factors, would yield the same power laws. What would change is the coefficients rather than the exponents. It was considered important to have these coefficients reasonably accurate in order to determine whether they were significantly influenced by metallurgical factors such as grain size. There are indications of such an effect, but the influence of grain size was not systematically investigated.

SUMMARY AND CONCLUSIONS

Dynamic fracture was studied in two hypereutectoid steels, FS-01 and HF-1, that easily shatter when loaded at explosive strain rates. The number and size distribution of particles generated by such a process is well-characterized by the Mott cumulative distribution function. The tendency for the fragments to coarsen with increasing metal ductility is a qualitative observation made here and elsewhere. The phenomenology of brittle fragmentation was examined and a simple model was developed based on the concept of crack branching phenomenology. The model was made quantitative by establishing relationships between the energies associated with crack branching and the Mott parameters that characterize the particle distribution. This model

predicts that the average mass of a particle in the shattered body is proportional to the fourth power of the K_B/K_{IC} ratio. K_H/K_{IC} was more convenient experimentally than K_B/K_{IC}. In subsequent experiments the dependence of the Mott parameters on K_H/K_{IC} agreed reasonably well with fourth power law, so long as there was a significant amount of radial fracture in the exploding cylinder. The most ductile condition of FS-01 steel produced results that were far out of line with predictions because the cylinders fragmented entirely by shear, which is contrary to the assumption of brittle fracture in the model; so this result is not surprising. However, it is noteworthy that static tensile elongation correlated monotonically with the Mott parameters for each material. Since these high-strength brittle steels are not particularly sensitive to strain rate, the dependence of these parameters on the ductility may be through a $K_I - \delta_{cod} - \%\ \varepsilon\ell$ type of functional, which would be different for each material. This is believed to be the first time that dynamic material properties were used to construct a model that quantitatively predicts the relative size distributions of debris in blast-loaded structures of different materials.

The microscopic fracture modes were shown to be essentially independent of strain rate throughout the spectrum from quasistatic to explosive (i.e., 10^{-4} to 10^{6} sec^{-1}), at least for tensile failures. This supports the fracture mechanics approach.

The energy approach used in this study may be more general than was implied by the restriction to brittle opening mode cracks. It should be possible, although much more difficult, to develop similar models for Mode II fractures. The case of failure by full-wall shear could then be handled and the mixed mode case made more accurate.

In reality, it is the fracture energy that dominates the break-up. The proposed crack branching modification to Mott's fragmentation model should be interpreted symbolically, rather than literally, because parallel cracks in close proximity to each other can propagate simultaneously only if they are both traveling at terminal velocity, or one will be arrested. Normally crack branching will occur. But more importantly, even if it doesn't, such contiguous cracks will experience stress intensities of the same order of magnitude as for microbranching. Therefore the energies will be the same as for the multiple branching events. After all, two very closely spaced terminal velocity cracks cannot yield intrinsically any information about their origins. Specifically, they cannot indicate whether they are branches of a former single crack or whether they nucleated independently. This aspect of the problem suggests a very general applicability of the method of analysis to all problems characterized by a multiplicity of finely spaced, high-velocity cracks.

Besides the obvious application of the present formalism to military fragmentation devices, it may be of value in studying the inverse problem of containment of accidental explosions without the

formation of hazardous high-energy fragments. Another area of practical technological significance to which this approach may be extended is the mechanics of rock fragmentation. By characterizing the particle size distributions in shattered structures of common rock in terms of explosive brisance or charge-to-mass ratio, it may be possible to specify the conditions necessary to produce a desired crater size or to produce average particle sizes which may be conveniently removed by commercial mining equipment. Along the same lines, the present formalism might be used to determine the most efficient impact energies for ore pulverization or mineral comminution. There are apparently many potential applications of crack branching methodology to fragmentation of brittle materials under dynamic loading conditions.

ACKNOWLEDGEMENTS

The authors are grateful to Prof. G.R. Irwin for helpful discussions on crack branching and fracture mechanics, and to Mr. J. Beetle for assistance with explosive testing of metals.

REFERENCES

1. Mott, N.F., "Fragmentation of Shell Cases," Proc. Roy. Soc. Lond., Series A189, pp. 300-308 (1947).

2. Weimer, R.J., and Rogers, H.C., "Crack Branching Stress Intensity and Fracture of Brittle Metals Under Explosive Loading," Proc. of the Second International Conference on the Mechanical Behavior of Materials, pp. 1473-1477, Boston, MA (1976).

3. Weimer, R.J., "The Fracture of Brittle Metals Under Explosive Loading," Ph.D. Dissertation, Drexel University, Philadelphia, PA (1977).

4. Anthony, S.R., Crack Branching in Metals, Ph.D. Thesis, Univ. of Newcastle-upon-Tyne (Sept. 1969).

5. Bardes, B.P., "Mechanism of Fragmentation of Silico-Manganese Steels," Report R-1918, Frankford Arsenal, Phila., PA (March 1969).

6. ASTM Standard E8-69, "Standard Methods of Tension Testing of Metallic Materials," American Society for Testing and Materials, Phila., PA (1969).

7. ASTM Standard E18-74, "Standard Test Methods for Rockwell Hardness and Rockwell Superficial Hardness of Metallic Materials, " American Society for Testing and Materials, Phila., PA (1974).

REFERENCES (continued)

8. ASTM Standard E399-74, "Standard Test Method for Plane-Strain Fracture Toughness of Metallic Materials," American Society for Testing and Materials, Phila., PA (1974).

9. Rinehart, J.S., and Pearson, J., Explosive Working of Metals, p. 150, The MacMillan Co., New York (1963).

10. Tada, H., Paris, P.C., and Irwin, G.R., The Stress Analysis of Cracks Handbook, Del. Research Corp., Hellertown, PA (1973).

11. Schardin, H., "Velocity Effects in Fracture," Fracture (B.L. Averbach, et al., eds.) M.I.T. Press, pp. 297-330, Cambridge, MA (1959).

12. Kerkhof, F., "Wave Fractographic Investigations of Brittle Fracture Dynamics," Dynamic Crack Propagation, pp. 3-35, Noordhoff, Leyden (1973).

13. Weimer, R.J., and Rogers, H.C., "A High-Speed Digital Technique for Precision Measurement of Crack Velocities," Fast Fracture and Crack Arrest, STP No. 627, ASTM, Phila., PA (1977).

14. Sih, G.C., and Irwin, G.R., "Dynamic Analysis for Two-Dimensional Multiple Crack Division," Eng. Fract. Mech., 1, pp. 603-614 (1970).

15. Freund, L.B., "Crack Propagation in an Elastic Solid Subjected to General Loading - II," J. Mech. Phys. Solids, 20, pp. 141-152 (1972).

16. Irwin, G.R., "Relatively Unexplored Aspects of Fracture Mechanics," T. & A.M. Rpt. No. 240, p. 31, Dept. of Theoretical & Applied Mechanics, Univ. of Illinois (1963).